Reentrant structural and optical properties of organic-inorganic hybrid metal cluster compound ((n-C4H9)(4)N)(2)[(Mo6Bri8Br6a)]

Norio Saito, Daiki Nishiyama, Yoshitaka Matsushita, Yoshiki Wada, Stéphane Cordier, Takeo Ohsawa, Fabien Grasset, Naoki Ohashi

COMMUNICATION

Reentrant Structural and Optical Properties of Organic–Inorganic Hybrid Metal Cluster Compound $((n\text{-}C_4H_9)_4N)_2[Mo_6Br^i_8Br^a_6]$

Received 00th January 20xx,
Accepted 00th January 20xx

DOI: 10.1039/x0xx00000x

Norio Saito,[a,b,†] Daiki Nishiyama,[a] Yoshitaka Matsushita,[a] Yoshiki Wada,[a,b] Stéphane Cordier,[c] Takeo Ohsawa,[a,b] Fabien Grasset,[a,b] Naoki Ohashi[a,b,d,e,*]

We report the reentrant phase transition of the organic–inorganic hybrid metal cluster (MC) compound $(TBA)_2[Mo_6Br^i_8Br^a_6]$ (TBA = $((n\text{-}C_4H_9)_4N)$). Structural studies revealed that $(TBA)_2[Mo_6Br^i_8Br^a_6]$ was crystallized in the conventional monoclinic phase with space group $P2_1/n$. When the crystal was cooled down to 143 K, we observed a structural phase transition from the conventional phase to an unknown phase with packing structure similar to the conventional one; however, the unit cell was extended to a double size. A reentrant transition to the conventional structure was induced when the crystal was further cooled to 113 K. These reentrant phase transitions occurred without any symmetry changes caused by slight motions of the MCs and TBA^+ ions. Luminescence studies revealed that the phase transition poorly affected the emission spectra; however, the newly found phase exhibited 1.7 times longer emission lifetime than the conventional phase. These results indicate that MC-based compounds are promising and exhibit phase transitions and crystallographic polymorphisms.

Hybrid crystallization of organic and inorganic molecular building blocks, that is, metal complexes, clusters, and organic molecules, is an effective strategy for creating functional organic–inorganic hybrid compounds with unique properties that are different from those of conventional all-inorganic compounds. Because these building blocks are associated with each other through weak intermolecular interactions such as van der Waals forces, hydrogen bonding, and coordinate covalent bonding, the hybrid crystals frequently exhibit excellent flexibility in the solid state [1] and unique ordered crystal structures [2−4], polymeric crystal frameworks [5], and their switching by external stimuli [6], which are the origin of several electronic and optoelectronic properties [7,8]. For example, Owczarek et al. investigated non-centrosymmetric low-weight molecular crystals comprising halogenated imidazole derivatives and their solid solutions, which exhibit ferroelectricity, piezoelectricity, and mechanical flexibility [9]. You et al. recently reported that a chloromanganese-based organic–inorganic hybrid-layered perovskite exhibits significantly large piezoelectricity similar to that of conventional barium titanate piezoceramics, because of the temperature-dependent structural phase transition triggered by the ordering and disordering of counter ammonium cations [10]. It should also be emphasized that fabricating thin films and single crystals of these compounds is possible using the solution process. This process facilitates the development of low-cost devices potentially used in information processing and electronic and optical applications. Hence, organic–inorganic hybrid crystals built with a combination of molecular building blocks have promising properties to circumvent some long-standing challenges in the field of conventional ceramic materials.

$[Mo_6X^i_8X^a_6]^{2-}$ (X = halogen) are known as functional metal clusters based units (MCs) suitable for constructing organic–inorganic hybrid compounds owing to their well-defined coordination structure and a wide range of interesting optical properties [11−13]. The molybdenum octahedron is stabilized by eight covalently bonded X^is and six ionically bonded X^as [14], providing a nano-scaled complex anion with a divalent negative charge. The negative charge of the MCs induces electrostatic association with both metal and organic cations such as cesium (Cs^+) and tetrabutylammonium (TBA^+) [15−18], thereby leading to the formation of ionic crystals with a long periodical range. In MC-based compounds, the counter cations generally occupy large interspaces formed by the anionic sublattice and are connected by hydrogen bonding via the X^a-sites and/or electrostatic interactions. Hence, there has been considerable interest in organic–inorganic hybrid MC-based compounds. For

[a] National Institute for Materials Science (NIMS), 1-1 Namiki, Tsukuba, Ibaraki 305-0044, Japan.
[b] CNRS–Saint-Gobain–NIMS, IRL 3629, Laboratory for Innovative Key Materials and Structures (LINK), National Institute for Materials Science, 1-1 Namiki, 305-0044 Tsukuba, Japan.
[c] Univ Rennes, CNRS, ISCR – UMR 6226, F-35000 Rennes, France.
[d] NIMS-Saint-Gobain Center of Excellence for Advanced Materials, NIMS, 1-1 Namiki, Tsukuba, Ibaraki 305-0044, Japan.
[e] Materials Research Center for Element Strategy (MCES), Tokyo Tech., 4259 Nagatsuta, Midori-ku, Yokohama 226-8503, Japan.
† Present address: Department of Industrial Chemistry, Faculty of Engineering, Tokyo University of Science, 1-3, Kagurazaka, Shinjuku, Tokyo 162-8601, Japan.
Electronic Supplementary Information (ESI) available: [details of any supplementary information available should be included here]. See DOI: 10.1039/x0xx00000x

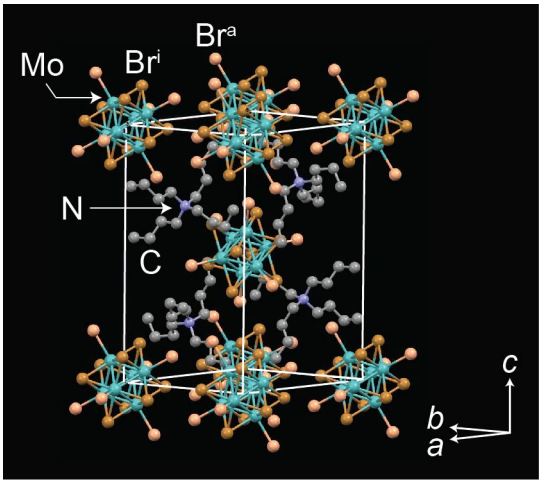

Figure 1. Crystal structure of $(TBA)_2[Mo_6Br^i_8Br^a_6]$ with the space group $P2_1/n$. Hydrogen atoms are not shown for clarity.

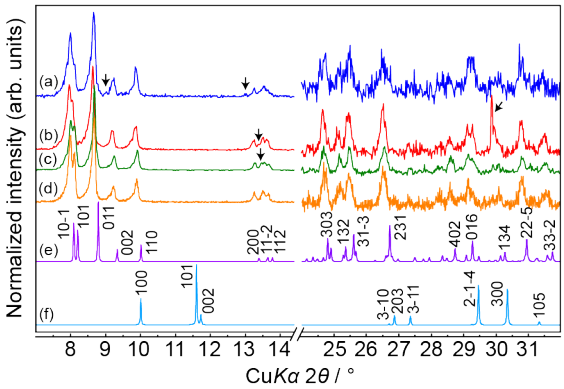

Figure 2. Powder XRD patterns of $(TBA)_2[Mo_6Br^i_8Br^a_6]$ recrystallized in (a) MeCN, (b) THF, (c) acetone, and (d) a mixture of acetone and EtOH. (e) and (f) are simulated ones for $(TBA)_2[Mo_6Br^i_8Br^a_6]$ and $Cs_2[Mo_6Br^i_8Br^a_6]$, respectively. Arrows presented in (a), (b), and (c) denote unidentified diffraction peaks. Every observed peak of (d) was indexable as the diffraction from $(TBA)_2[Mo_6Br^i_8Br^a_6]$ with the lattice parameters of a = 13.285 Å, b = 11.914 Å, c = 18.964 Å, and β = 90.957° belonging to the space group $P2_1/n$.

instance, novel optical and electronic functionalities could be exploited thanks to their structural diversity and the possibility of phase transitions. The tunability of structural arrangements and phase transitions are favored by the possibility of substitution on the X^a-site and reorientational motions of counter organic cations.

In this context, we explored the structural and optical properties of MC-based compounds containing molecular organic components. In a previous study [19], we reported that high concentrations of solvent molecules, such as dichloromethane and methanol, are entrapped by the interstitial sites of $Cs_2[Mo_6Cl^i_8Cl^a_6]$, which re-invokes easy insertion of the solvent molecules with the MCs during crystal growth operations. The present study focuses on the crystallization of high-purity MC-based compounds to understand their intrinsic structures and optical properties. As a result, we found that a typical MC-based organic–inorganic hybrid compound, $(TBA)_2[Mo_6Br^i_8Br^a_6]$, shows interesting phase transition behavior at low temperatures. Based on the crystallographic studies on $(TBA)_2[Mo_6Br^i_8Br^a_6]$, Kirakci et al. have already reported that the compound crystallizes in the monoclinic phase with the space group $P2_1/n$ (phase I) at both 293 and 100 K [15,16], as displayed in Fig. 1. However, we have discovered that the conformations and relative positions of the MC unit and TBA^+ cation were slightly reoriented in the intermediate temperature range (143 K), resulting in a structural transition to an unknown superlattice phase (phase II) without symmetry breaking. The crystal structure retained the conventional phase I at both higher (e.g., 203 K) and lower (e.g., 113 K) temperatures. Interestingly, this reentrant phase transition simultaneously prolonged the luminescence lifetime by 1.7 times. Herein, we investigate and report the reentrant phase transition of $(TBA)_2[Mo_6Br^i_8Br^a_6]$ using single-crystal X-ray diffraction (SCXRD) and demonstrate how the structural change affects its luminescence properties. Our findings will open the door for exploring the structural versatility and new properties of MC-based compounds.

For the preparation of $(TBA)_2[Mo_6Br^i_8Br^a_6]$, $Cs_2[Mo_6Br^i_8Br^a_6]$ was synthesized using a previously reported method [15]. Subsequently, the Cs^+ cation was substituted by the TBA^+ cation in a 50/50 ethanol (EtOH)/H_2O mixture, as described in the SI. Because the pristine sample included some impurity phase(s), it was purified by recrystallization in dehydrated solvents. Figure 2 shows powder X-ray diffraction (XRD) profiles of the samples recrystallized in acetonitrile (MeCN), tetrahydrofuran (THF), acetone, and a mixture of acetone/EtOH. The profiles indicate that these procedures successfully yielded single-phase $(TBA)_2[Mo_6Br^i_8Br^a_6]$ crystallized in a well-known crystalline form, as reported in previous studies [15,16]. No trace of residual phase was found in XRD patterns, indicating that cationic exchange between Cs^+ and TBA^+ was completed. By comparing the XRD patterns, it can be seen that recrystallization in MeCN, THF, and acetone caused peak splitting and/or small humps which could not be indexed as diffraction from $(TBA)_2[Mo_6Br^i_8Br^a_6]$. For example, small humps were observed at 2ϑ = 9.02° and 13.02° in the profile for the specimen recrystallized in MeCN (Fig. 2a). Similarly, the diffraction peaks for the sample recrystallized in THF and acetone at around 2ϑ = 13–14° (Fig. 2b,c) showed splitting into more than four peaks. Those results were inconsistent to the simulated profile of $(TBA)_2[Mo_6Br^i_8Br^a_6]$ (Fig. 2e). The diffraction profile for the specimen recrystallized in THF also showed an unknown sharp peak at 2ϑ = 29.88°. These unidentified peaks were possibly due to a secondary phase involved in solvation of $(TBA)_2[Mo_6Br^i_8Br^a_6]$. Indeed, MeCN was reported to be easily solvated with metal clusters [20]. Since single phase sample, without any trace of resudual phases were obtained by recrystallization in acetone/EtOH (Fig. 2d), we concluded that recrystallization in acetone/EtOH was suitable for the preparation of single crystal with better crystallinity and less contamination. Subsequently, we performed structural and optical characterizations of $(TBA)_2[Mo_6Br^i_8Br^a_6]$ using single crystals purified by recrystallization in an acetone/EtOH solvent.

The crystal structure of $(TBA)_2[Mo_6Br^i_8Br^a_6]$ was analyzed by SCXRD performed at 113–300 K (see Table S1 for the results of the structure refinements at 203, 143, and 113 K). When we

assumed the known crystal structure of $(TBA)_2[Mo_6Br^i_8Br^a_6]$ (phase I), the refinements of the diffraction intensities obtained at 203 and 113 K were well converged ($R_1 \approx 4$–6.5%, $e \approx 1.0$–2.5 e Å^{-3}). While the structure refinement at 143 K was also well converged without serious electron residues, the intensity data indicated a new phase that had double-sized unit cell volume compared to phase I. Following discussion describes details in crystal structures determined by these refinements.

The refined lattice parameters are listed in Table S2. The parameters observed at 203 K resulted in a = 13.136(1) Å, b = 11.763(1) Å, c = 18.975(1) Å, β = 90.737(1)°, and V = 2931.6(2) Å^3, which is known to be phase I. However, the lattice parameters observed at 143 K (phase II) were significantly different from those observed at 203 K. As shown in Table S2, good convergence of the structural refinement was achieved when a super-lattice structure was assumed. The refined lattice parameters of phase II were a = 22.820(3) Å, b = 11.989(2) Å, c = 22.879(3) Å, β = 111.912(4)°, and V = 5807.2(13) Å^3. It is noteworthy that the cell volume of phase II was exactly two times larger than that of phase I, as transformable to a cell (a = 12.792 Å, b = 11.989 Å, c = 18.933 Å, and β = 89.841°) identical to that of phase I using a transformation matrix $P = (\frac{1}{2}0\frac{1}{2}/010/\frac{1}{2}0\frac{1}{2})$. This transformation also suggested that phase II can be regarded as a (pseudo)orthorhombic phase. The normalized unit cell volume (i.e., the cubic root of the volume) observed at each temperature (Fig. S1) shows good consistency with the linearity of thermal expansion (α = 63.34×10^{-6} K^{-1}), thus implying that the structural change induced little expansion/shrinkage of the crystal structure.

The double-sized unit cell of phase II is due to the small rotation and displacement of the MC unit and TBA^+ cation. The ORTEP diagram of the two crystal phases is shown in Fig. S2 illustrates a definite difference in the rotational angle of the MC unit and conformation of the tetrabutyl groups of the TBA^+ cation. Here note that the structure refinements revealed that a few C atoms (C14 and C33 for 203 K and C14 for 143 K) were disordered at 143 and 203 K. Indeed, the refined isotropic ADPs, B_{iso}, listed in Tables S3 and S4 show that the ADPs for the C atoms resulted in particularly high values compared to those of the MC unit, which were indicative of active thermal motions of the TBA^+ cation.

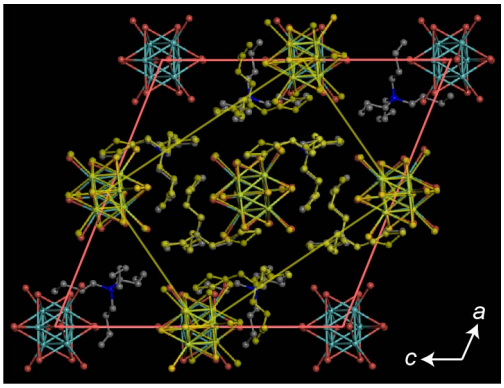

Figure 3. Projection viewing of the crystal structure of $(TBA)_2[Mo_6Br^i_8Br^a_6]$ refined at 203 K (phase I) and 143 K (phase II). The unit cell of phase I represented with semi-transparent yellow color is overlaid on that of phase II represented in red color. This figure indicates that rotational orientation of the MC unit and displacement of TBA^+ caused the phase transition.

A comparison between the crystal structures of phases I and II is presented in Fig. 3. The crystal structure of phase I at 203 K represented by a yellow unit cell shows that the MCs centered at (0, 0, 0) are lined-up in a single inclination pattern viewed from the ac plane. The tetrabutyl groups of the TBA^+ cations formed a square-hook pattern surrounding the MC. In contrast, when the crystal structure is transformed to phase II at 143 K (represented as a red unit cell in Fig. 3), the MC units become slightly rotated, resulting in two inclination patterns alternatively arranged over the ac plane. In addition to the rotational motions of the MC unit, the molecular conformation and relative positions of the tetrabutyl groups of the TBA^+ cation are also displaced. The rotational motions and conformational displacements of these building blocks increase the number of asymmetric molecules in the unit cell, thereby resulting in a double-sized unit cell in the crystal structure of phase II. The coordination environments surrounding the MC anion are shown in Fig. S3, indicating that the minimum interatomic distances of the H and Br atoms were in the range of 2.85–2.99 Å. Since the typical bond length of the H–Br hydrogen bond is 2.6 Å [21], the MC and TBA^+ ions are predominantly associated through electrostatic interactions.

In order to trace thermal anomalies accompanied with the phase transition, differential scanning calorimetry (DSC) measurement of $(TBA)_2[Mo_6Br^i_8Br^a_6]$ was performed from 103 to 298 K. As shown in Fig. 4, a pair of endothermic and exothermic signals was observed at 181 K and 171 K in each heating and cooling cycle, corresponding to the phase transition between phase I and phase II. The thermal hysteresis of 10 K suggests that this phase transition was first-order type. Peak area analysis revealed that entropy change (ΔS) of this phase transition calculated by the equation $\Delta S = \Delta H/T$ was 18.5 J K^{-1} mol^{-1} for heating and 13.5 J K^{-1} mol^{-1} for cooling. According to Boltzmann equation $\Delta S = R \ln(N)$, where R is the gas constant, and N is the fraction of the number of geometrical distinguishable states in phase I and II, the value of N for heating was calculated to be N = 9.2, indicating that order–disorder of the constituent atoms should involve the phase transition. Significant increase of the N value in phase I was accounted for by disorder of the TBA^+ cations as discussed above. Additionally, note that present DSC measurements could not detect clear thermal changes at lower temperature side. The absence of thermal anomaly at lower transition temperature was attributed to limitation of the sensitivity of DSC instrument, as our set up using liquid-N_2 as coolant was not appropriate for measurements at such low temperature.

Figure 5a shows the photoluminescence (PL) spectra of the $(TBA)_2[Mo_6Br^i_8Br^a_6]$ crystal in the temperature range of 100–210 K. A broad emission centered at 788 nm was observed at 100 K and exhibited a blue shift with increasing temperature. According to a previous study [22], this luminescence blue shift originates in the zero-field splitting of emissive triplet states. Figure 5b shows the time-resolved photoluminescence (TRPL) spectra of the compounds measured at 100, 160 and 210 K. In this figure, the slope of the luminescence decay is reflected in

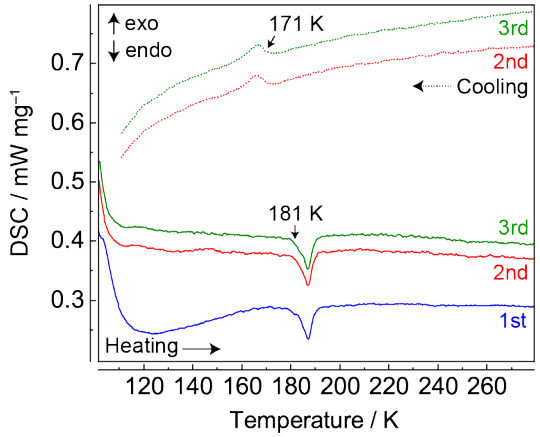

Figure 4. DSC profiles of $(TBA)_2[Mo_6Br^i_8Br^a_6]$ for three heating and cooling cycles, measured from 103 to 298 K. Temperatures denoted in the plot indicate onset points of the observed endothermic or exothermic peak.

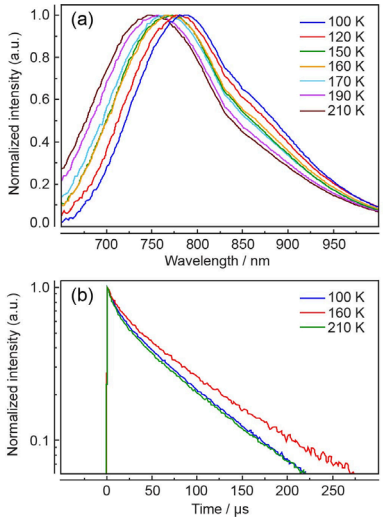

Figure 5. (a) PL and (b) TRPL spectra of $(TBA)_2[Mo_6Br^i_8Br^a_6]$ observed at 100, 160, and 210 K in the solid state. The PL spectra were blue-shifted with increasing temperature owing to the zero-field splitting of emissive triplet states. The spectrum shape slightly changed owing to the temperature changes. In contrast, the TRPL curve measured at 160 K exhibited a gentler slope compared to other curves, thereby indicating prolongation of the PL lifetime at 160 K.

the magnitude of the PL lifetime (τ). Moreover, the decays at 100 and 210 K were very close; however, that at 160 K clearly showed gentler slopes. Figure S4 that depicts the TRPL spectra over 100–210 K indicated that decline of the TRPL curve was enhanced at 100 K and in 190–210 K. This characteristic seems to be correlated with the temperature-dependent structural changes observed by SCXRD and DSC. It is noteworthy that the decay of the TRPL curve was maximally reduced at 170 K, which was almost identical to the phase transition temperature observed by DSC. In addition, decline of the TRPL curve was remarkably reduced by heating from 100 to 110 K, suggesting that the phase transition was assumed to be evoked. We approximated the value of τ from the curve fitting of the TRPL spectra by assuming an exponential decay component (i.e., $I(t) = I_0e^{-t/\tau}$). The results of the curve fitting shown in Table S5 indicate that the values of τ at 100 and 210 K were equal and calculated to be 180 μs. However, the τ value observed at the intermediate temperature, e.g., at 160 K further extended to τ = 300 μs. Assuming that the intrinsic radiative decay of $[Mo_6Br^i_8Br^a_6]^{2-}$ was constant [23], the extended PL lifetime suggested that radiative decay became more dominant by the inhibition of non-radiative processes.

The above measurements revealed that $(TBA)_2[Mo_6Br^i_8Br^a_6]$ exhibited a temperature-induced reentrant phase transition accompanied by a significant prolongation of its PL lifetime. Here, we discuss the possible origins of these behaviors. In general, a class of crystalline compounds comprising alkylammonium cations often undergo one or more phase transitions. This is because their high-temperature phases are generally associated with the freedom of rotational and reorientational motions of the alkylammonium cations [24,25]. In MC-based compounds, a phase transition of $(TBA)_2[W_6Cl^i_8Cl^a_6]$, similar to the present study, has already been reported by Johnston et al. [26]. This study reveals that $(TBA)_2[W_6Cl^i_8Cl^a_6]$ undergoes a structural transition from the $P2_1/n$ unit cell at room temperature to the $P2_1/c$ double-sized cell at 268 K. The structural refinement of $(TBA)_2[W_6Cl^i_8Cl^a_6]$ performed at 150 and 200 K indicate very close similarity between the packing arrangements of the room- and low-temperature cells and disorder of the hydrocarbon chain for one of the TBA^+ cations in these cells. The rotational angle of the $[W_6Cl^i_8Cl^a_6]^{2-}$ anion and the relative positions and conformations of the TBA^+ cations resemble those of $(TBA)_2[Mo_6Br^i_8Br^a_6]$, but are not completely identical. In addition, the literature did not mention whether the unit cell of $(TBA)_2[W_6Cl^i_8Cl^a_6]$ could exhibit a reentrant transition to the half-size cell at temperatures lower than 150 K. Therefore, the $(TBA)_2[M_6X^i_8X^a_6]$ compound system could commonly exhibit a phase transition between the already known $P2_1/n$ phase and double-sized $P2_1/c$ phase, originating in the motions of the MC and TBA^+ ions in a low temperature range. However, the reentrancy of the structural transition is specific to the $(TBA)_2[Mo_6Br^i_8Br^a_6]$ compound system.

With temperature dependency of luminescence properties for MC-based compounds, Kitamura et al. [20] reported that the luminescence lifetime of $(TBA)_2[Mo_6Cl^i_8Cl^a_6]$ was approximately 200 μs at 100 K and monotonically decreased with increase in temperature. Thus, it seems that the reentrant characteristics of the luminescence lifetime is specific to $TBA_2[Mo_6Br^i_8Br^a_6]$. Interestingly, the literature reported that $(TEA)_2[Mo_6Cl^i_8Cl^a_6]$ (TEA = tetraethylammonium) exhibited significantly longer luminescence lifetime than that of the TBA salt in entire temperature range (e.g., $\tau \approx 250$ μs at 100 K), suggesting that packing arrangement of the MC units affects the luminescence property. From those discussion, we concluded that the reentrant change of the PL lifetime should be involved by the phase transition between the conventional and double-size cells.

To understand the reentrant transition of the crystal structure and investigate the luminescence properties of $(TBA)_2[Mo_6Br^i_8Br^a_6]$, we calculated the formation enthalpies of phases I and II using density functional theory. The computational results showed that the difference in the formation enthalpies of both unit cells was less than 0.02 eV

(Table S6), thereby suggesting that they are comparable at 0 K. Thus, we assume that the phase transition of $(TBA)_2[Mo_6Br^i_8Br^a_6]$ would not be significantly associated with the enthalpic effect, but with the entropic effect. Indeed, we observed disorder of the C atoms in the crystal structures at 143 and 203 K. Moreover, the isotropic ADPs summarized in Tables S3 and S4 indicated particularly small B_{iso} values for the C atoms refined at 143 K. Interestingly, they were significantly smaller than those at 113 K refined by the present study and those at 100 K reported in the literature [16], although atomic motions in solid states are generally reduced at lower temperatures. This indicates that the packing arrangement of phase II is characteristic of suppressing the thermal motions of the TBA^+ cations. We assume that the atomic motions and disorder of the packing arrangement would contribute to an increase in the entropy of phase I, and then the packing arrangement of phase I would stabilize at 113 K. In addition, the enhancement of the PL lifetime in phase II is rationalized because the atomic motions of the TBA^+ cations were particularly reduced.

In summary, herein, we investigated the impurity-free crystal growth of $(TBA)_2[Mo_6Br^i_8Br^a_6]$ and its crystallographic characterization at different temperatures. The results revealed that the compound underwent a reentrant phase transition between the already known $P2_1/n$ phase observed at 113 K and 203 K and a double-sized $P2_1/c$ super lattice observed at 143 K. We highlight that the phase transition to the double-sized lattice exhibited a significantly longer PL lifetime (τ = 300 μs) compared to previously reported ones [27]. This is indicative of an enhancement in the luminescence efficiency along with the structural transition. There have been a few studies that have investigated the phase transitions and crystallographic polymorphs of MC-based compounds [26]. Therefore, this study is the first to discover the reentrancy of the phase transition and improvement of the optical property by the crystal structure change in the MC-based compound system; meanwhile this study still remained some structure and property investigations such as temperature-variable measurements of powder XRD and photoluminescence quantum yield, and those will be vital to further understand the present phenomena. The phase transition of $(TBA)_2[Mo_6Br^i_8Br^a_6]$ is associated with the rotational and reorientational motions of the MC and TBA^+ ions. Therefore, hybrid crystallization between the MCs and alkylammonium cations is promising for providing further structural diversity and new functionalities characteristic of non-centrosymmetric structures such as piezoelectricity and ferroelectricity. Hence, we will continue the crystallographic investigations and explore the functionalities of these family compounds in the future.

Acknowledgement

The majority of this work was performed under the France–Japan international collaboration framework (IRL-LINK). The authors thank those involved in LINK and its related activities, particularly David Lechevalier and Mari Kono of Saint-Gobain KK (Tokyo, Japan) for their contributions to the management of LINK. We thank Noée Dumait and Serge Paofai of ISCR for their contributions to the synthesis of $Cs_2[Mo_6Br^i_8Br^a_6]$. N.S. would also like to thank Prof. Junzo Tanaka of Tokyo Tech for their support and encouragement. Parts of this study were financially supported by Saint-Gobain Company (Paris, France) and CNRS. This study was also supported by the Ministry of Education, Culture, Sports, Science and Technology via the Elemental Strategy initiative.

Conflicts of interest

There are no conflicts to declare.

Notes and references

Crystallographic information (Cif) data of $(TBA)_2[Mo_6Br^i_8Br^a_6]$ refined at 113, 143, and 203 K have been deposited at the Cambridge Crystallographic Data Centre (CCDC), under deposition numbers CCDC 2113791, 2097143, and 2097144.

1 V. Jella, S. Ippili, J.-H. Eom, S. V. N. Pammi, J.-S. Junga, V.-D. Tran, V. H. Nguyen, A. Kirakosyan, S. Yun, D. Kim, M. R. Sihn, J. Choi, Y.-J. Kim, H.-J. Kim, and S.-G. Yoon, *Nano Energy*, 2019, **57**, 74–93.
2 C. C. Stoumpos, D. H. Cao, D. J. Clark, J. Young, J. M. Rondinelli, J. I. Jang, J. T. Hupp, and M. G. Kanatzidis, *Chem. Mater.*, 2016, **28**, 2852−2867.
3 H. Li, M. Eddaoudi, M. O'Keeffe, and O. M. Yaghi, *Nature*, 1999, **402**, 276−279.
4 A. M. Champsaur, A. Velian, D. W. Paley, B. Choi, X. Roy, M. L. Steigerwald, and C. Nuckolls, *Nano Lett.*, 2016, **16**, 5273−5277.
5 W.-H. Zhang, Z.-G. Ren, and J.-P. Lang, *Chem. Soc. Rev.*, 2016, **45**, 4995−5019.
6 F.-L. Hu, H.-F. Wang, D. Guo, H. Zhang, J.-P. Lang, and J. E. Beves, *Chem. Commun.*, 2016, **52**, 7990−7993.
7 H. L. B. Boström, M. S. Senn, and A. L. Goodwin, *Nat. Commun.*, 2018, **9**, 2380.
8 M. I. Saidaminov, O. F. Mohammed, and O. M. Bakr, *ACS Energy Lett.*, 2017, **2**, 889−896.
9 M. Owczarek, K. A. Hujsak, D. P. Ferris, A. Prokofjevs, I. Majerz, P. Szklarz, H. Zhang, A. A. Sarjeant, C. L. Stern, R. Jakubas, S. Hong, V. P. Dravid, and J. F. Stoddart, *Nat. Commun.*, 2016, **7**, 13108.
10 Y. M. You, W.-Q. Liao, D. Zhao, H.-Y. Ye, Y. Zhang, Q. Zhou, X. Niu, J. Wang, P.-F. Li, D.-W. Fu, Z. Wang, S. Gao, K. Yang, J.-M. Liu, J. Li, Y. Yan, and R.-G. Xiong, *Science*, 2017, **357**, 306−309.
11 P. Kumar, S. Kumar, S. Cordier, S. Paofai, R. Boukherroub, and S. L. Jain, *RSC Adv.*, 2014, **4**, 10420−10423.
12 A. Renaud, F. Grasset, B. Dierre, T. Uchikoshi, N. Ohashi, T. Takei A. Planchat, L. Cario, S. Jobic, F. Odobel, and S. Cordier, *ChemistrySelect*, 2016, **1**, 2284−2289.
13 D. G. Nocera and H. B. Gray, *J. Am. Chem. Soc.*, 1984, **106**, 825−826.
14 N. Saito, S. Cordier, P. Lemoine, T. Ohsawa, Y. Wada, F. Grasset, J. S. Cross, and N. Ohashi, *Inorg. Chem.*, 2017, **56**, 6234−6243.
15 K. Kirakci, S. Cordier, and C. Perrin, *Z. Anorg. Allg. Chem.*, 2005, **631**, 411−416.
16 K. Kirakci, S. Cordier, T. Roisnel, S. Golhen, and C. Perrin, *Z. Kristallogr. NCS*, 2005, **220**, 116−118.
17 P. Bruckner, W. Preetz, and M. Punjer, *Z. Anorg. Allg. Chem.*, 1997, **623**, 8−17.
18 W. Preetz and D. Bublitz, *Z. Anorg. Allg. Chem.*, 1994, **620**, 234−246.

19 N. Saito, P. Lemoine, S. Cordier, Y. Matsushita, T. Ohsawa, F. Grasset, J. S. Cross, and N. Ohashi, *Z. Anorg. Allg. Chem.*, 2021, **647**, 1−9.
20 N. Kitamura, Y. Kuwahara, Y. Ueda, Y. Ito, S. Ishizaka, Y. Sasaki, K. Tsuge, S. Akagi, *Bull. Chem. Soc. Jpn.* 2017, **90**, 1164–1173.
21 Y.-Y. Zhu, H.-P. Yi, C. Li, X.-K. Jiang, and Z.-T. Li, *Cryst. Growth Des.,* 2008, **8**, 1294−1300.
22 H. Miki, T. Ikeyama, Y. Sasaki, and T. Ammi, *J. Phys. Chem.*, 1992, **96**, 3236−3239.
23 T. C. Zietlow, M. D. Hopkins, and H. B. Gray, *J. Solid State Chem.*, 1985, **57**, 112−119.
24 W. Trigui, A. Oueslati, F. Hlel, and A. Bulou, *J. Raman Spectrosc.*, 2017, **48**, 1718−1724.
25 X.-G. Chen, J.-X. Gao, X.-N. Hua, and W.-Q. Liao, *New J. Chem.*, 2018, **42**, 14909−14913.
26 D. H. Johnston, C. M. Brown, A. S. Yu, and J. C. Gallucci, *Acta Cryst.*, 2010, **C66**, m303−m306.
27 M. Amela-Cortes, A. Garreau, S. Cordier, E. Faulques, J.-L. Duvailb, and Y. Molard, *J. Mater. Chem. C*, 2014, **2**, 1545−1552.

